Advanced Robotics, 2013
Vol. 27, No. 9, 725–738, http://dx.doi.org/10.1080/01691864.2013.779052

Taylor & Francis
Taylor & Francis Group

FULL PAPER

Gas source localization with a micro-drone using bio-inspired and particle filter-based algorithms

Patrick P. Neumann[a]*, Victor Hernandez Bennetts[b], Achim J. Lilienthal[b], Matthias Bartholmai[a] and Jochen H. Schiller[c]

[a]*BAM Federal Institute for Materials Research and Testing, Berlin, D-12205, Germany;* [b]*Mobile Robotics and Olfaction Lab, AASS Research Center, Örebro University, Örebro, SE-70182, Sweden;* [c]*Institute of Computer Science, FU University, Berlin, D-14195, Germany*

(*Received 3 September 2012; accepted 28 November 2012*)

Gas source localization (GSL) with mobile robots is a challenging task due to the unpredictable nature of gas dispersion, the limitations of the currents sensing technologies, and the mobility constraints of ground-based robots. This work proposes an integral solution for the GSL task, including source declaration. We present a novel pseudo-gradient-based plume tracking algorithm and a particle filter-based source declaration approach, and apply it on a gas-sensitive micro-drone. We compare the performance of the proposed system in simulations and real-world experiments against two commonly used tracking algorithms adapted for aerial exploration missions.

Keywords: autonomous micro UAV; chemical and wind sensing; gas source localization; particle filter

1. Introduction

Airborne gas source localization (GSL) is important for leakage detection on geodynamically active regions, waste disposals, landfill sites, and carbon capture and storage (CCS) areas. The vast majority of approaches that have been proposed for GSL take inspiration from insects and other simple life forms. Insects have the outstanding ability to find distant sources of odors by tracking wind-borne odor plumes to their emission source.[1] In an analogous way, robots try to mimic their plume tracking behavior to reach the source, where they declare the end of their task.[2] Insects and other animals that have inspired robotics research for gas plume tracking include: moths, which use odor localization to find mates,[3] lobsters, which locate food through chemical sensing,[4] *Escherichia coli* bacteria, which use odor localization to find nutrients,[5] and dung beetles, which use odor localization to find hatching niches and food.[5] Bio-inspired algorithms are generally based on two principles: *chemotaxis* and *anemotaxis*. *Chemotaxis* refers to a mechanism in which the movement of an organism (or robot) is determined by the gas distribution, most often by the concentration gradient. *Anemotaxis* instead refers to a mechanism in which the movement of an organism (or robot) is determined by the sensed airflow (or fluid flow).

In addition, engineering approaches for GSL have also been proposed. Vergassola et al. [6], for example, presented a search strategy called 'infotaxis'. Infotaxis is based on probability and information theory, and was designed to work in turbulence-dominated environments. The location of the source is modeled as a probability distribution which is derived from previously collected concentration measurements. The robot tries to reduce the entropy of the modeled distribution by moving to neighboring locations for which a high information gain is expected.

To the author's knowledge, implementations of these algorithms have been tested and evaluated exclusively on ground-based robot platforms, autonomous underwater vehicles (AUV), and blimps. Ground-based robots cannot reach the emission source in certain cases due to, e.g., obstacles or rough terrain. Blimps, on the other hand, are highly affected by the wind and have a bad size-to-payload proportion. To overcome the constraints of ground-based robots and blimps, we propose a quickly deployable, flying mobile measurement device based on a quadrocopter.

This work deals with the problem of GSL in natural environments with a quadrocopter-based micro-drone. The rotors of the micro-drone induce disturbances, which heavily affect the gas distribution. Ground-based mobile robots could be operated at very low speeds, which affect the gas distribution only marginally in comparison to a micro-drone. Thus, the task of GSL becomes even more challenging when being airborne. Furthermore,

*Corresponding author. Email: Patrick.Neumann@bam.de

most experiments have been performed under simplified conditions, such as a steady constant airflow and the presence of a single gas source emitting a known chemical compound at a constant release rate. However, the airflow in an open outdoor environment is turbulence-dominated [7] creating complex structures of gas patches with different concentration levels. To the author's knowledge, it is the first time that this task is accomplished with an airborne micro-drone in real-world scenarios.

This paper is structured as follows, we first present in Section 2 a gas-sensitive micro-drone that is the basis for the real-world experiments performed in this work, including a novel approach to estimate the wind vector based on the micro-drone's onboard sensors. Next, we discuss three bio-inspired plume tracking algorithms for a gas-sensitive micro-drone in more detail (Section 3): the surge-cast algorithm (a variant of the silkworm moth algorithm),[8] the zigzag/dung beetle algorithm,[9] and a newly developed algorithm called 'pseudo gradient-based algorithm'. The latter includes a new measuring strategy to deal with the strong disturbances induced by the rotors of the micro-drone – measuring a local concentration gradient with spatially separated sensors is in this case not feasible. The task of declaring the source is still an open issue rarely addressed in the past. This work provides an integral solution for the GSL task, by incorporating gas source declaration with a novel particle filter (PF)-based approach (Section 4). We compare the performance of the algorithms in simulation and real-world experiments with each other (Sections 5 and 6), draw conclusions, and identify directions of future work (Section 7).

2. Design of the gas-sensitive micro-drone

2.1. Robotic platform

The Airrobot AR100-B micro-drone (Airrobot GmbH & Co. KG, Germany, in this article referred to as micro-drone) has a diameter of 1 m and is driven by four brushless electric motors (Figure 1(a)). The maximum payload mass amounts to 200 g with a total flight mass of about 1.3 kg. The onboard LiPo battery allows a flight time of up to 30 min. The micro-drone can withstand a maximum wind speed of $8\,\mathrm{ms}^{-1}$. The micro-drone can be operated manually or in Global Positioning System (GPS) mode, e.g., by autonomous waypoint following with a step size of $\geqslant 1$ m. The flight control relies on an onboard inertial measurement unit (IMU), which also provides the basis for the wind vector estimation presented in Section 2.4. The IMU consists of a three axis accelerometer and a three axis rotation rate sensor. Magnetic field sensor (compass) and GPS improve the accuracy of the IMU, and are used to compensate for the sensor drift. In addition, a barometric pressure sensor is used to control the altitude of the micro-drone. Communication with the ground station is established by a wireless radio link. Data packets can include control instructions or data coming from the micro-drone's onboard sensors. The operating distance of the remote control and communication link is 1 km.

2.2. Gas-sensing payload

The micro-drone was modified to incorporate gas-sensitive devices as payloads (Figure 1(b)). An configurable electronic nose (e-nose) – specially adapted to the micro-drone at AASS, Örebro University – and a commercially available gas detector (Dräger X-am 5600, Dräger Safety AG & Co. KGaA, Germany) were used as gas-sensitive payloads. The e-nose is capable of accommodating up to four commercially available metal oxide sensors and one electrochemical cell. The Dräger gas detector can measure many combustible gases and vapors with a catalytic sensor as well as different (toxic) gases with electrochemical and infrared sensors. In total, the Dräger gas detector is capable of accommodating simultaneously four gas sensors. The e-nose allows a sampling rate of

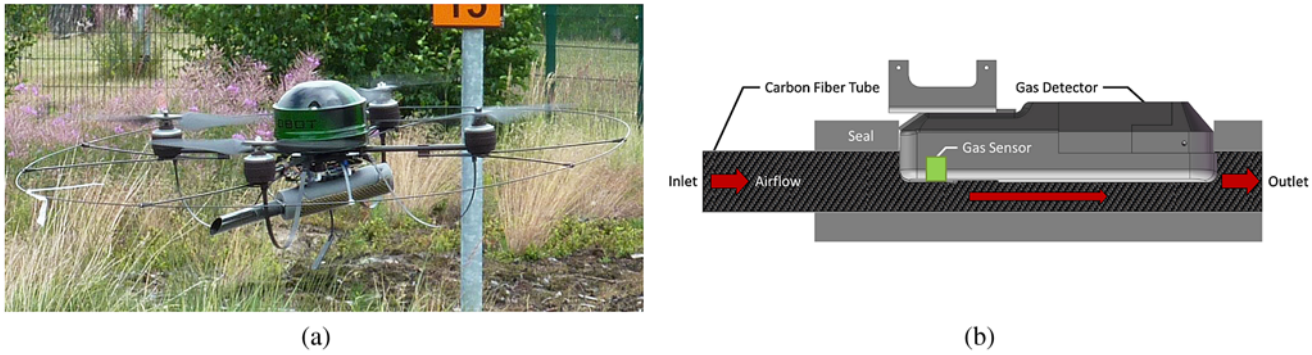

(a) (b)

Figure 1. (a) Airrobot AR100-B micro-drone equipped with gas-sensitive payload and (b) schematic diagram of the gas-sensitive payload: gas detector attached to the gas transport housing (side view). (For the colour version of this figure, please see the online article: http://dx.doi.org/10.1080/01691864.2013.779052.)

8 Hz for each sensor, whereas the Dräger gas detector allows a sampling rate of 1 Hz for each sensor.

2.3. Gas transport to the sensors

Gas transport to the sensors is a critical process due to the induced disturbance by the rotors of the micro-drone, which basically dilutes and disperses the surrounded gas–air mixture. This could be problematic for scenarios where punctual gas sources are present or the gas sensors work at the lower limit of detection. However, as shown in [10], measurement of gas concentration in large volumes is feasible for gas-sensitive micro-drones.

To improve the measurement capabilities for small plumes, we present in [11] different design approaches that lead to less diluted gas–air mixture at the gas sensors. They were implemented and analyzed with respect to their functional performance. The results of the validation experiments show that conveying the downwards directed airflow of one rotor through a carbon fiber tube to expose the sensors with the surrounded gas–air mixture gives the best results regarding applicability and sensitivity (Figure 1(b)). Using this gas transport approach is also advantageous as the effective sensor response and decay can be sped up to some degree by the artificially generated airflow to achieve faster and more accurate gas concentration measurements with shorter residence time of the micro-drone.

2.4. Estimation of the wind vector

Wind information is of high importance for gas-sensitive robots. For example, the steering trajectories of anemotaxis plume tracking algorithms are based on wind measurements. However, due to the restrictions imposed by the platform, the micro-drone does not carry any dedicated wind sensor. Instead, we proposed in [11] a method that can be used to estimate the wind vector by fusing the micro-drone's onboard sensors to compute the parameters of the wind triangle.

The wind triangle is commonly used in aerial navigation and describes the relationships between the flight vector $\vec{v} = (r_v, \theta_v)$, the ground vector $\vec{w} = (r_w, \theta_w)$, and the wind vector $\vec{u} = (r_u, \theta_u)$, where r denotes the length and θ the directional component of the vectors. Two of the three vectors or four of the six parameters of the wind triangle are needed in order to derive the remaining parameters. However, only the ground vector $\vec{w}$ is directly given by the GPS receiver of the micro-drone. We calculate the flight speed r_v by using a reference function computed from a set of wind tunnel measurements. Additionally, the orientation information coming from the onboard compass is used to compute the flight direction θ_v. Finally, the wind vector $\vec{u}$ is computed from the wind triangle by applying the law of cosines.

3. Gas source localization (GSL)

The task of localizing a gas source can be broken down into three subtasks [2]: (1) plume acquisition (find the plume), (2) plume tracking (move the robot reactively along/within the plume), and (3) source declaration (predict the most likely location of the emitting source).

The first two algorithms presented in this section use only binary gas information from one sensor, i.e., they either detect the presence/absence of the target gas. To obtain this binary value, the average measured gas concentration is thresholded (th_c). Using binary gas information helps to mitigate calibration issues with the gas sensors. The third algorithm uses directly the measured concentrations from two spatially separated measuring positions of one sensor. However, more sophisticated algorithms could be used to detect the presence/absence of the target gas.

The micro-drone was programmed to stop at each measuring position to collect gas sensor and wind measurements for a prolonged time (here: 20 s). Finally, the collected measurement data are averaged over the measurement time at each measurement point.

3.1. Plume acquisition phase

Possible plume acquisition strategies to make contact with the plume are passive monitoring of the environment and active exploration strategies. A passive strategy (waiting for the plume) is not feasible for a flying, high power-consuming micro-drone. Instead, an active exploration strategy has to be used, for example, a randomized or systematic search.

In this work, the micro-drone was programmed to follow a *sweeping* trajectory, i.e., the micro-drone makes a step orthogonal to the wind direction as long as the plume is not found. One step in upwind direction (or search direction) is made and sweeping direction is inverted, if the micro-drone would leave the search area. When the plume is found, the micro-drone switches to plume tracking.

3.2. Plume tracking phase

3.2.1. Surge-cast algorithm

Lochmatter presented in [8] the *surge-cast* algorithm. It is a combination of plume tracking strategies used by the silkworm moth and works as follows (Figure 2(a)): The robot moves straight upwind until it looses the contact with the plume for a certain distance d_{lost}. Then, it tries to reacquire the plume by searching crosswind for a defined distance d_{cast} on both sides. The chance of reacquiring the plume in the first crosswind movement is maximized by measuring the wind direction to estimate the side from which the robot has left the plume. Every

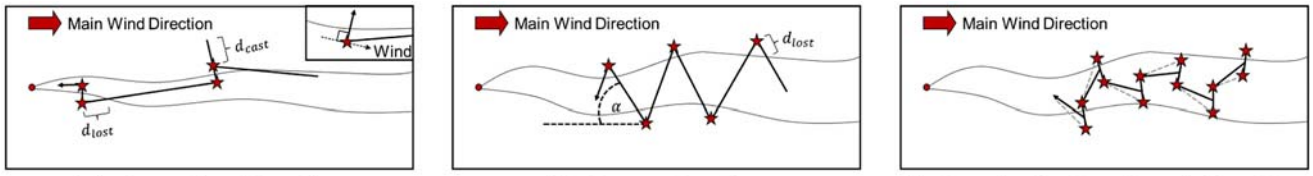

(a) Surge-Cast Algorithm (b) Zigzag Algorithm (c) Pseudo Gradient-based Algorithm

Figure 2. Illustration of (a) the surge-cast algorithm introduced by Lochmatter [8], (b) the zigzag algorithm introduced by Ishida et al. [9], and (c) the pseudo-gradient-based algorithm. The stars indicate the positions where the wind direction is measured. In (a) and (b) the gas concentration is measured permanently, whereas the gas concentration in (c) is only measured at the indicated measuring positions. The gray dotted line is the flight path of the micro-drone. (For the colour version of this figure, please see the online article: http://dx.doi.org/10.1080/01691864.2013.779052.)

time the robot switches its behavior from upwind surge to casting and vice versa, the wind direction is re-measured.

In comparison to the original algorithm, the plume is declared lost in the surge-cast algorithm used here when the micro-drone measures an average gas concentration below the threshold after one step. To reacquire the plume, casting with increasing step size in crosswind direction is performed. These changes were necessary to address the constraints of the micro-drone in GPS mode. Furthermore, the wind is re-measured for iteration of the algorithm to adapt faster to changing wind conditions. If casting fails to reacquire the plume (after a defined number of steps), the micro-drone returns to the sweeping strategy.

3.2.2. *Zigzag/dung beetle algorithm*

The zigzag or dung beetle algorithm was first reported by Ishida et al. [9]. The basic algorithm works as follows (Figure 2(b)): The robot moves upwind with an angle α (e.g., $\alpha = 60^{\circ}$) across the plume constantly sensing gas concentrations. If the gas sensor measures a concentration below a given threshold th_c, the robot is assumed to have reached the edge of the plume. It re-measures the wind direction and continues moving upwind with an angle $-\alpha$ with respect to the upwind direction. This procedure is repeated causing the robot to move in a zigzag fashion within the plume. The robot is stopped, when it has reached the source.

In comparison to the original algorithm, the micro-drone does only collect gas and wind measurements at the waypoints where it stops.

3.2.3. *Pseudo-gradient-based algorithm*

The idea for the first gradient-based algorithms for plume tracking goes back to Braitenberg [12]. The chemical gradient is measured by a pair of bilateral gas sensors mounted on each side of a robot, each directly controlling the speed of a wheel. Each sensor is connected to the motor on the same side, the motor on the opposite side (cross-coupling), or both motors. Although it was a purely chemotactic approach, a Braitenberg-style robot is able to track a plume towards a gas source by following the concentration gradient.[13]

As the first gradient-based algorithms do not consider wind information, the robot does not know whether it is following a plume towards or away from its source. Turning the robot in proportion to the concentration gradient in dependence of the upwind direction solves this problem.[5]

As the rotors of the micro-drone introduce strong disturbances, measuring a local concentration gradient with spatially separated sensors is not feasible. Instead a new measuring strategy was developed, which basically splits up one measuring position into two spatially separated ones. In order to respect the minimum step size of the micro-drone of 1 m and to progress faster to the source, the step size in upwind direction was set to 1.5 × step size.

The pseudo-gradient-based algorithm consists of the following steps (Figures 2(c) and 3): The micro-drone collects gas sensor and wind measurements at position p_1 and makes a step orthogonal to the wind direction. The direction of the first crosswind step is given by the current sweeping direction. At position p_2 the gas concentration and the wind is re-measured. Next, the

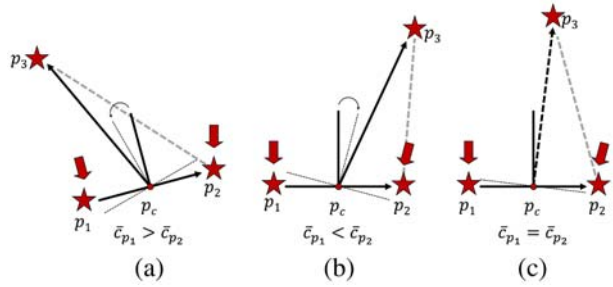

Figure 3. Three different cases of the gradient-based algorithm: (a) $\bar{c}_{p_1} > \bar{c}_{p_2}$, (b) $\bar{c}_{p_1} < \bar{c}_{p_2}$, and (c) $\bar{c}_{p_1} = \bar{c}_{p_2}$. The case $\bar{c}_{p_1} = \bar{c}_{p_2} = 0$ restarts the plume acquisition phase. The red stars indicate the measuring positions, the red arrows illustrate the averaged wind directions, and the gray dotted line is the flight path of the micro-drone. (For the colour version of this figure, please see the online article: http://dx.doi.org/10.1080/01691864.2013.779052.)

concentration gradient is calculated based on the averaged gas concentrations $\bar{c}_{p_1}$ and $\bar{c}_{p_2}$ collected at position p_1 and position p_2 (an average concentration below the threshold is set to zero):

$$grad(\bar{c}_{p_1}, \bar{c}_{p_2}) = \frac{\bar{c}_{p_1}}{\bar{c}_{p_1} + \bar{c}_{p_2}},\ grad(\bar{c}_{p_1}, \bar{c}_{p_2}) \in [0, 1] \quad (1)$$

The new measuring position p_3 is calculated based on the concentration gradient $grad(\bar{c}_{p_1}, \bar{c}_{p_2})$ and the center position p_c (Figure 3):

$$grad(\bar{c}_{p_1}, \bar{c}_{p_2}) \begin{cases} >0.5, & \delta = (\bar{\theta}_u)_{p_1} + \beta \cdot 2 \cdot (grad(\bar{c}_{p_1}, \bar{c}_{p_2}) - 0.5) \quad \text{(Figure 3(a))} \\ <0.5, & \delta = (\bar{\theta}_u)_{p_2} + \beta \cdot 2 \cdot (1 - grad(\bar{c}_{p_1}, \bar{c}_{p_2}) - 0.5) \quad \text{(Figure 3(b))} \\ = 0.5, & \delta = (\bar{\theta}_u)_{p_1,p_2} \quad \text{(Figure 3(c))}, \end{cases} \quad (2)$$

where δ denotes the azimuth direction angle, β is the maximum possible upwind angle, and $(\bar{\theta}_u)_{p_1,p_2}$ is the wind direction averaged over the wind data collected at both measuring positions. If $grad(\bar{c}_{p_1}, \bar{c}_{p_2}) > 0.5$, the upwind angle β is set to $-\beta$ and the direction of the crosswind movement is inverted. Finally, the micro-drone flies directly to position p_3 and repeats with the first step. If $\bar{c}_{p_1} = \bar{c}_{p_2} = 0$, the micro-drone returns to sweeping with changed sweeping direction.

3.3. Source declaration

In recent work, source declaration was mainly established by reaching a predefined proximity to the known location of the gas source with the mobile robot. This was commonly performed visually by a human observer.[2] First approaches without human interaction were suggested, e.g., in [14,15]. For example, Li sent his REMUS AUV on cloverleaf trajectories to estimate the source location.[15]

More recently Li et al. proposed in [16] a GSL algorithm based on a PF. It estimates the location of the gas source in real-time, while the robot performs an exploratory behavior in an outdoor environment with time-variant airflows. They use a likelihood function in combination with a gas patch path reconstruction approach to calculate a so-called observation window. The observation window defines the area where the robot assumes to be the origin of the gas patch. In case of a detection event, particles are added and spread out in the observation window. Finally, the collected information is exploited by the PF algorithm, which terminates if all particles converged in one point within a certain radius. Li et al. evaluated their algorithm in 33 real-world experiments. However, a disadvantage of this algorithm is that it assumes a roughly uniform airflow over the search space.

In contrast to the PF-based GSL algorithm presented in [16], we introduce a novel PF-based algorithm based on a PF that not only use gas-detection events to estimate the location of a gas source. Furthermore, our proposed approach does not rely on a roughly uniform wind field, which in the real-world does not exist. Instead, measured wind data, more precisely mean and variance of the wind, were included in the proposed approach as indicator for the wind stability.

4. PF-based GSL algorithm

In this work, we introduce a new source declaration algorithm based on a PF. It uses gas and wind measurements to reconstruct the trajectory of a gas patch since it was released by the gas source until it reaches the measurement position of the micro-drone to estimate the gas source location. Because of the turbulent nature of the wind, the uncertainty in the wind direction is included in the computation process by creating a patch path envelope (PPE) instead of a single patch trajectory. The PPE describes the envelope of an area the gas patch has passed with high probability. The source is considered to be found, if the location estimate remains within a small region for a defined number of iterations.

First, we describe the preprocessing of the sensor data (Section 4.1). Next, we show how the PPE is constructed (Section 4.2). Sections 4.3 and 4.4 describe the update and resampling step of the PF algorithm. Section 4.5 describes how the location of the gas source is estimated based on the particle set.

4.1. Sensor data preprocessing

4.1.1. Gas sensor

To decide whether the micro-drone was within the plume or not, a binary concentration measure z_t with an adaptive

threshold $\bar{c}_t$ is used as proposed by Li et al. [16]. This binary concentration measure is defined as:

$$z_t = \begin{cases} 1, & \text{if } c_t > \bar{c}_{t-1} \\ 0, & \text{otherwise} \end{cases} \tag{3}$$

with

$$\bar{c}_t = \begin{cases} \lambda \bar{c}_{t-1} + (1-\lambda) c_t, & \text{if } t \geq 1 \\ c_t, & \text{if } t = 0, \end{cases} \tag{4}$$

where c_t is the measured gas concentration of one sensor averaged over the measurement interval at iteration t, c_0 is the initial gas concentration detected at the start of the algorithm, and $\lambda \in [0, 1]$. $z_t = 1$ indicates a gas-detection event, whereas a nondetection event is represented as $z_t = 0$. As proposed in [16], λ is set to 0.5 during all experiments to respond correctly and in time to all gas-detection events.

4.1.2. Wind sensor

At each iteration t, the averaged wind direction $\bar{\theta}_u$ and the circular variance S_0 are computed from a set of single wind measurements taken at the current measuring position. Here, the circular variance is used to consider the nonregularities of the wind flow direction in the construction process of the PPE.

4.2. Construction of the PPE

For the construction of the PPE we assume to collect wind measurements with the micro-drone in turbulent real-world environments with nonuniform wind fields. The PPE describes the envelope of the most probable area where the gas patch has passed. The opening angle of the PPE depends on the degree of stability of the wind direction. Stable wind conditions result in small opening angles, whereas unstable and changing wind conditions result in large opening angles.

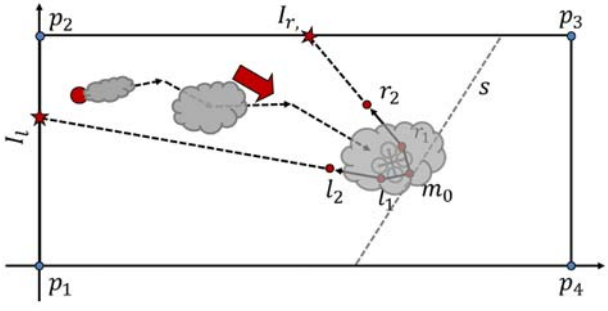

Figure 4. Construction of the PPE for the micro-drone in real-world environments in nonuniform wind fields. The source location is denoted by the large red dot. The measurement radius of the micro-drone is modeled as a simple triangle given by the positions m_0, l_1, and r_1. The search area is defined by the four points p_1 to p_4. (For the colour version of this figure, please see the online article: http://dx.doi.org/10.1080/01691864.2013.779052.)

The left and right paths of the PPE are calculated using the great circle navigation formulae.[17] The positions l_2 and r_2 are determined based on the positions l_1 and r_1 and the azimuth direction angles δ_l and δ_r (Figure 4). The azimuth direction angles δ_l and δ_r are calculated as follows:

$$\delta_{l,r} = (\bar{\theta}_u \pm 90^\circ \cdot S_0) \bmod 360^\circ \tag{5}$$

To consider the measurement radius of the micro-drone due to the rotor movement and to achieve numerical stability during stable wind conditions (e.g., the possibility of overlaying line segments in the beginning of the paths in case of zero circular variance), the first segment of the PPE is modeled as a simple triangle with its right angle rotated in downwind direction based on the averaged wind measurements.

Finally, the PPE C_t is constructed anticlockwise by adding the vertex m_0, r_1, the intersection point I_r, all corner points of the area border in between the intersection points, the intersection point I_l, l_1, and m_0 to close the PPE. The output of this stage is the PPE C_t (Figure 4).

4.3. Update step of the PF

The update phase calculates for each particle $x_t^{[i]}$ of the particle set $\mathcal{X}_t$ the new importance weight $\omega_t^{[i]} \in \Omega_t$ based on the previous importance weight $\omega_{t-1}^{[i]} \in \Omega_{t-1}$, the PPE C_t, and the binary concentration value z_t. Particles within the PPE are processed differently than particles that lie outside the PPE. Furthermore, a straight line s orthogonal to the averaged wind direction is defined that goes through vertex m_0 (Figure 4). Now, the particles are classified in one of the following three classes: (a) particles located *inside* the PPE, (b) particles located *outside* of the PPE in upwind direction with respect to line s, and (c) particles located *outside* the PPE in downwind direction with respect to line s. Then, the following function is used to update the corresponding importance weights:

$$\begin{aligned} \omega_t^{[i]} &= f(x_t^{[i]}, \omega_{t-1}^{[i]}, C_t, z_t) \\ &= \begin{cases} \omega_{t-1}^{[i]} & \forall x_t \in (\text{a}) \wedge z_t = 1 \\ \alpha \cdot \frac{\theta_{C_t}}{180^\circ} \cdot \omega_{t-1}^{[i]} & \forall x_t \in (\text{b}) \wedge z_t = 1 \\ \alpha^2 \cdot \frac{\theta_{C_t}}{180^\circ} \cdot \omega_{t-1}^{[i]} & \forall x_t \in (\text{c}) \wedge z_t = 1 \\ \beta^2 \cdot \frac{\theta_{C_t}}{180^\circ} \cdot \omega_{t-1}^{[i]} & \forall x_t \in (\text{a}) \wedge z_t = 0 \\ \beta \cdot \omega_{t-1}^{[i]} & \forall x_t \in (\text{b}) \wedge z_t = 0 \\ \omega_{t-1}^{[i]} & \forall x_t \in (\text{c}) \wedge z_t = 0 \end{cases} \end{aligned} \tag{6}$$

where α and β are meta-parameters, which adjust the contribution of the old importance weight $\omega_{t-1}^{[i]}$ of particle $x_t^{[i]}$ at iteration t to the new importance weight $\omega_t^{[i]}$ and $\theta_{C_t} \in (0180]^\circ$ is the opening angle of the first segment of the PPE (and not of the triangle). The classification of the particles is implemented by the square of α and β, respectively. By introducing the term $\theta_{C_t}/180^\circ$ in Equation (6), an additional punishment of particles is allowed in dependency of the stability of the wind. Small opening angles reflect stable wind conditions. In case of a detection event, it is assumed that the gas source is located within the PPE as the measured gas was released by the source and transported by the wind forming a plume. Thus, it is very unlikely that particles which are located outside the PPE reflect the gas source location. Accordingly, these particles can be punished additionally. In case of a nondetection event, it is assumed that the gas source is not located within the PPE, which allows further punishment of these particles as well. On the other hand, large opening angles indicate unstable wind conditions. Here, it is not possible to limit the large number of possible source locations as the origin of the measured concentration is more uncertain. Therefore, the punishment of the particles should be much lower or should be even omitted.

4.4. Resampling step of the PF

One problem which can occur using PF algorithms is the degeneration of particles, i.e., most of the importance weights have negligible weights. The effective sample size $\hat{N}_{eff}$ can be used to monitor whether *resampling* is necessary [18] and can be approximated as:

$$\hat{N}_{eff} = \frac{1}{\sum_{i=1}^{N} (\omega_t^{[i]})^2}, \tag{7}$$

where $\omega_t^{[i]}$ is the normalized importance weight of particle $x_t^{[i]}$. If the effective sample size $\hat{N}_{eff}$ drops below a given threshold (here: $N/2$) *resampling* should take place, i.e., eliminating particles with small importance weights and duplicating the particles with larger importance weights.

4.5. Estimation of the gas source location

The particles set $\mathcal{X}_t$ can be used to estimate the location of the gas source $\bar{x}_s$. A simple strategy could be to calculate the weighted mean over all particles. However, observations have shown that the weighted mean is often not a good estimator since it is strongly affected by outliers (which in addition occur frequently as a consequence of resampling). Furthermore, it is very unlikely that all particles will converge in one certain point considering the turbulent nature of the wind.

A more sophisticated strategy involves analyzing the particle clusters that have evolved over time. The proposed strategy searches the particle $x_t^{[k]}$ with the highest number of neighbors within a certain radius ε, i.e., the k for which

$$|\{x_t^{[j]} \,|\, \forall j \in [1, N] \wedge k \neq j : |x_t^{[k]} - x_t^{[j]}| \leqslant \varepsilon\}|$$

is maximized. In the current implementation, ε is set to 0.5 m. This particle $x_t^{[k]}$ is called the maximum neighbors estimate (MNE) and used as the gas source location estimate.

5. Simulation experiments

Simulations were performed in order to determine the performance and robustness of each plume tracking algorithm under repeatable conditions. The performance is measured as the distance overhead, which is defined as the ratio between the travelled distance of the micro-drone and the upwind distance to the gas source. This performance metric was introduced in [8] and indicates what distance the robot had to move in order to come 1 m closer to the source (the value is therefore greater than or equal to one). One practical advantage of this metric is that the results are independent from the starting position of the micro-drone. The robustness is defined as the success rate of the algorithm.

In order to evaluate the performance of the PF-based GSL algorithm, the parameters $\alpha \in [0.1, 1.0]$ and $\beta \in [0.1, 1.0]$ are optimized in simulations with respect to the average localization error and the success rate for data-sets collected with the pseudo-gradient-based algorithm. The localization error is defined as the distance between the true gas source location and the estimate described in Section 4.5. Here, the success rate is defined as the ratio of successful localizations, in which the localization error is less or equal than 1.5 m, with respect to the total number of performed experiments.

As a simulation environment, we use the filament-based gas dispersion model developed by Pashami et al. [19]. In addition, we developed a sensor model in analogy to the one presented in [20]. The sensor response is modeled as an exponential rise and decay using experimental sensor data. The positioning system error of the micro-drone is modeled as vector with samples of a zero-mean normal distribution with σ^2 set to 1.17 (the value was obtained from real-world experiments). To model the disturbances of the rotors on the measurements, the gas concentration values are simply averaged at the measurement position within a radius of 0.5 m before applying the gas sensor model. The wind sensor is modeled as a perfect sensor with the option to add noise to the directional component. The noise is added

using samples of a zero-mean normal distribution ($\mathcal{N}(0, \sigma_\theta^2)$) with variable σ_θ^2.

5.1. Experimental setup

The experimental area is a simulated wind tunnel with the size $32 \times 8\,\mathrm{m}^2$. The flow speed in the wind tunnel was set set to $0.5\,\mathrm{ms}^{-1}$. A circular gas source with a radius of 0.2 m was placed in the experimental area at position (2, 4) m. The gas source releases 500 filaments per second, which are uniformly distributed over the circular area of the source.[19] In each run, the micro-drone was started inside the plume at position (31, 4) m. The step size was set to 1 m. The measuring time at each sampling location was set to 20 s with a sampling frequency of 1 Hz and the threshold th_c was set to 0.05 (the concentration data were normalized to one before usage). The parameter α of the zigzag algorithm and the parameter β of the pseudo-gradient-based algorithm were successively set to 15°, 30°, 60°, and 75° (zigzag) and 30°, 60°, and 90° (gradient). The wind sensor noise σ_θ^2 was variable during all sets of experiments and a total of 100 runs were performed for each value of σ_θ^2 .

A run was considered successful, if the micro-drone reached a $1.5 \times 2\,\mathrm{m}^2$ large area centered in front of the source, and unsuccessful, if the robot touched an arena wall or passed the target area. This stop criterion was chosen as the step size constraint of $\geq$1 m does not permit the micro-drone to track a small scale plume. The plume width at the source location has approx. the same width as the source itself (here: $\varnothing = 0.4$ m). Therefore, it is most likely that the micro-drone jumps over the plume without detecting a concentration level above the threshold. This is also the reason why larger step sizes of the micro-drone were not investigated.

The same experimental setup was used to optimize the meta-parameters for the PF algorithm with the following exceptions: The source was located at position (8, 4) m and only the gradient-based algorithm with β set to 90° was used as control algorithm. To model the lower limit of detection of the modeled gas sensor, the threshold th_c was used as well. The number of particles was set to 1000. The wind sensor noise σ_θ^2 was set to 14.02 and the noise $\sigma_{S_0}^2$ to calculate the circular variance S_0 was set to 23.08. Both values correspond to the characteristics of the micro-drone and were obtained from real-world experiments,[10,11] i.e., the proposed algorithm is optimized especially for the used robotic platform and its measuring capabilities and characteristics. The experiment was repeated 100 times.

5.2. Experimental results

A total of 5600 runs were performed for the three plume tracking algorithms. A sample trajectory of a successful run for each algorithm can be seen in Figure 5.

The results of the surge-cast algorithm are shown in Figure 6(e). The performance of this algorithm is fairly

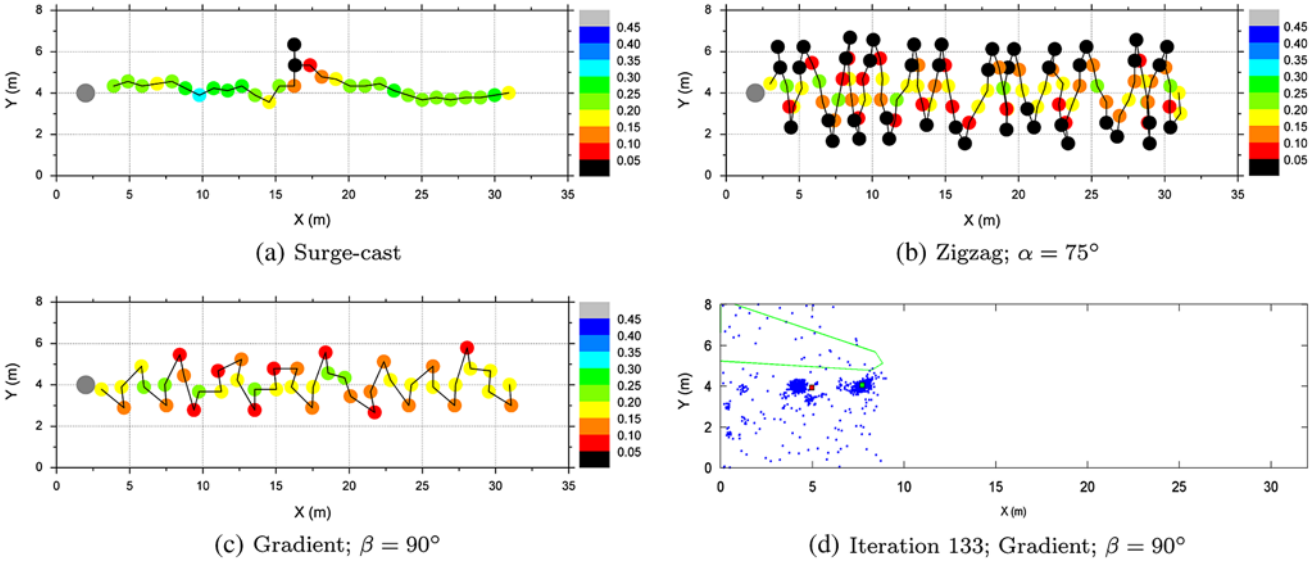

Figure 5. (a)–(c) Trajectories of successful simulation runs of all three bio-inspired plume tracking algorithms with $\sigma_\theta^2 = 14.02$. The source is indicated with the large gray circle. The smaller colored circles show the measured concentration at the sampling locations. (d) Particles (blue points) of the PF-based GSL algorithm using the pseudo-gradient-based tracking algorithm after 133 iterations. The estimated gas source location is indicated by the green point that corresponds to the MNE. The location of the true gas source is hidden by the green point. The red point denotes the prediction of the weighted mean. The PPE for a nondetection event is indicated by the green line. (For the colour version of this figure, please see the online article: http://dx.doi.org/10.1080/01691864.2013.779052.)

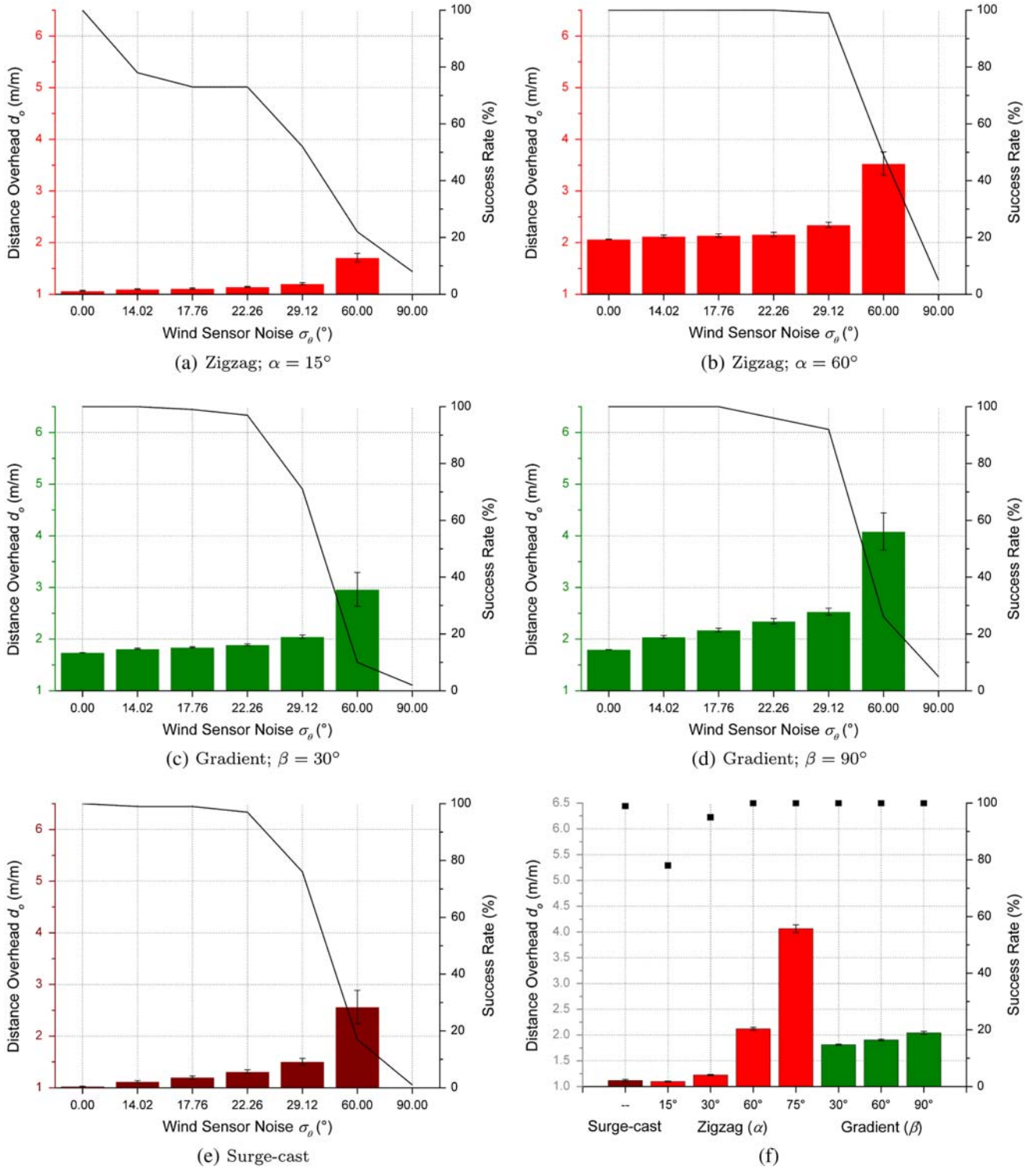

Figure 6. Simulation results obtained for the different bio-inspired plume tracking algorithms: the zigzag algorithm with α set to (a) 15° and (b) 60°, the pseudo-gradient-based algorithm with β set to (c) 30° and (d) 90°, and (e) the surge-cast algorithm. The error bars indicate the 95% confidence interval for the mean (assuming normally distributed data). The last bar is omitted in each bar plot because of the small number of successful runs. (f) Comparison of the obtained simulation results of all three algorithms with $\sigma_\theta^2 = 14.02$. The error bars indicate the 95% confidence interval for the mean. (For the colour version of this figure, please see the online article: http://dx.doi.org/10.1080/01691864.2013.779052.)

good. The distance overhead of the algorithm is ≤ 1.5 for $\sigma_\theta^2 \leq 29.12$ and it seems that the wind sensor noise has only a small influence on the performance of the algorithm as long as the error does not exceed $\sigma_\theta^2 > 29.12$. However, the wind sensor noise highly affects the success rate.

Figure 6(a) and (b) present the results of the zigzag (casting) algorithm for $\alpha = 15^\circ$ and 60°. The performance of this algorithm heavily depends on its parameter α (upwind angle): small upwind angles result in a small distance overhead but also in a low success rate, whereas a large angle increases significantly the success rate and the distance overhead at the same time as the micro-drone has to turn more often at the plume boundaries to stay within the plume. Thus, the upwind angle α presents a tradeoff between robustness and performance of this algorithm and has to be chosen carefully. Again it seems that the wind sensor noise has only a marginal influence on the performance of the algorithm.

The results of the pseudo-gradient-based algorithm are presented in Figure 6(c) and (d) for $\beta = 30^\circ$ and 90°. The parameter β has only a minor influence on the performance and the success rate of the algorithm. β should not be chosen too small as a small angle probably prevents the micro-drone to reacquire the plume if lost. The wind sensor noise seems to affect mainly the success rate of the algorithm.

Figure 6(f) shows the obtained simulation results of all three algorithms with $\sigma_\theta^2 = 14.02$ in a summary. It can be seen that the zigzag algorithm with $\alpha = 15^\circ$ and the surge-cast algorithm have the best distance overhead, followed by the zigzag algorithm with $\alpha = 30^\circ$. The results of the pseudo-gradient-based algorithm lies in the medium range, followed by the zigzag algorithm with $\alpha = 60^\circ$ and 75°. Therefore, the zigzag algorithm with $\alpha = 15^\circ$ and 30° and the surge-cast algorithm are the most performant algorithms within this comparison, but also the least robust ones. Even with a small wind sensor error of only $\sigma_\theta^2 = 14.02$, they are not able to reach success rates of 100%. High robustness and reasonable distance overheads are given by the pseudo-gradient-based algorithm and the zigzag algorithm with $\alpha = 60^\circ$. The zigzag algorithm with $\alpha = 75^\circ$ offers the highest robustness, but produces the worst distance overhead in this comparison.

Lochmatter [8] also performed 1350 simulated runs for pure casting (zigzag), surge-spiraling, and surge-casting using comparable simulation environment. Unfortunately, a gradient-based algorithm was not considered in Lochmatter's comparison. However, our results for the surge-cast and zigzag algorithm are comparable with the results he obtained.

Figure 7 shows the dependency of the source localization accuracy on the meta-parameters for the gradient-based control algorithm with β set to 90° after the last measurement point for the gas source located at position $(8, 4)$ m. In general, it stands out that the average localization error drops significantly with increasing β. On the other hand, the average localization error increases with increasing α. Thus, it seems to be beneficial to choose a small value for α and a large value for β. This means that, in case of a gas-detection event, the particles which are located *outside* the PPE are penalized much harder (in dependency of their relative position to line s with α or α^2) than, in case of a nondetection event, the particles which are located in upwind direction of line s (which are penalized in dependency of their relative position to the PPE with β or β^2). This position-

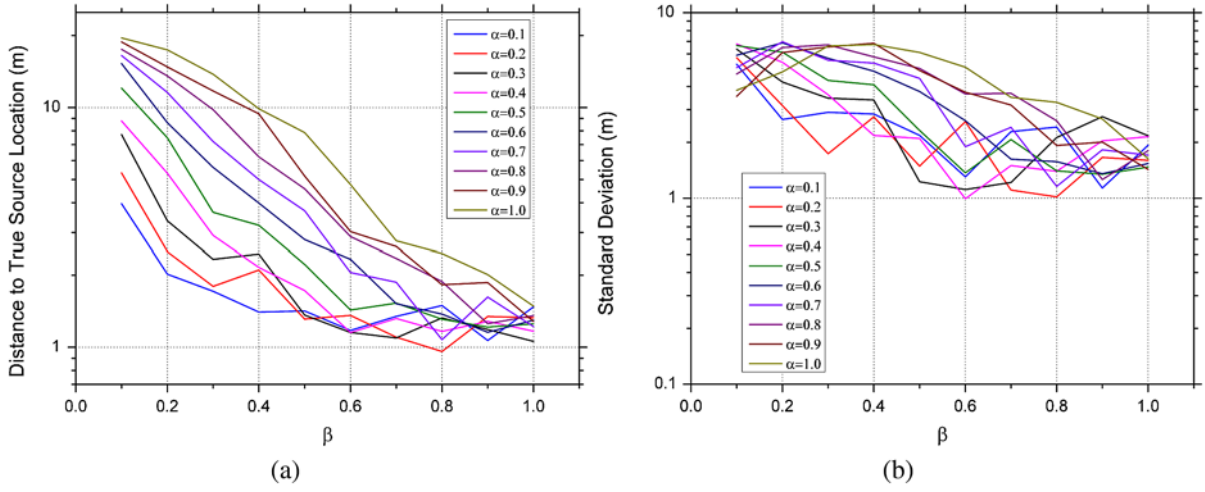

Figure 7. Dependency on the meta-parameters of the PF-based GSL algorithm for the gradient-based control algorithm. Note that the plots are created using a linear scale for the x-axis and a base 10 logarithmic scale for the y-axis for better data representation. (For the colour version of this figure, please see the online article: http://dx.doi.org/10.1080/01691864.2013.779052.)

dependent punishment of the particles allows them to accumulate at the location of the gas source and its close proximity.

A good parameter set for the gradient-based algorithm which minimizes the average localization error and maximizes the success rate is found to be $(\alpha, \beta) = (0.2, 0.8)$. The average error in the simulations with this parameter set was only $0.96\,\text{m} \pm 1.01\,\text{m}$ with a success rate of 86% (the average error of succssful localizations is $0.62 \pm 0.37\,\text{m}$).

6. Real-world experiments

6.1. Experimental setup

All plume tracking experiments were carried out in the outdoor environment shown in Figure 8 with the micro-drone equipped with the e-nose as gas-sensing payload. The e-nose was equipped with a single Figaro TGS2611 gas sensor, which is highly sensitive to methane (CH_4). A CH_4 gas cylinder was placed in a $20 \times 16\,\text{m}^2$ large area approx. at position $(3.2, 5.7)$ m from the bottom left corner. The outlet of the gas source was extended with a small tube, which was attached to a fan in order to spread the analyte away from the cylinder. The air current introduced by the fan also prevented the CH_4 to immediately rise up to the atmosphere when released. The step size of the micro-drone was set to 1.5 m for the surge-cast and the pseudo-gradient-based algorithm and 2.0 m for the zigzag algorithm, respectively, and the flight speed between the measurement positions was set to $1\,\text{ms}^{-1}$. The parameter of the zigzag algorithm was set to 60° in the first and 75° in the second run. The parameter of the pseudo-gradient-based algorithm was set to 60°. The corresponding algorithm was activated directly after take-off.

6.2. Experimental results

Figure 9(a)–(c) show the trajectories produced by the micro-drone and Table 1 shows the experimental results. The plume acquisition phase and starting positions were excluded from the evaluation to make the results rudimentary comparable with each other. Particularly noticeable are the runs #2 (surge-cast) and #6 (gradi-

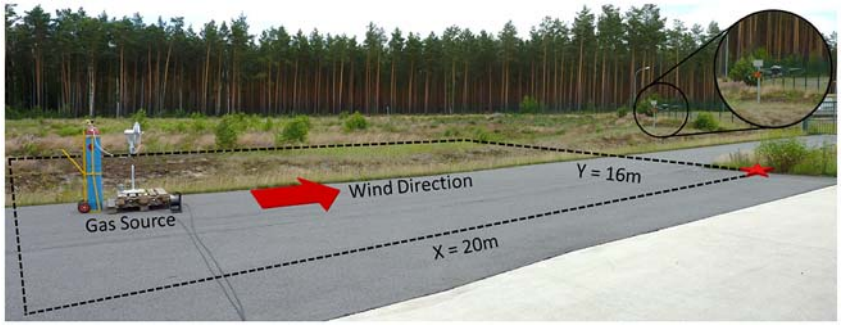

Figure 8. Setup of the plume tracking experiments. The red arrow illustrates the main wind direction during the experiments. The start position of the micro-drone is indicated by the red star. The micro-drone can be seen in the image enlargement in the upper right corner of the figure. (For the colour version of this figure, please see the online article: http://dx.doi.org/10.1080/01691864.2013.779052.)

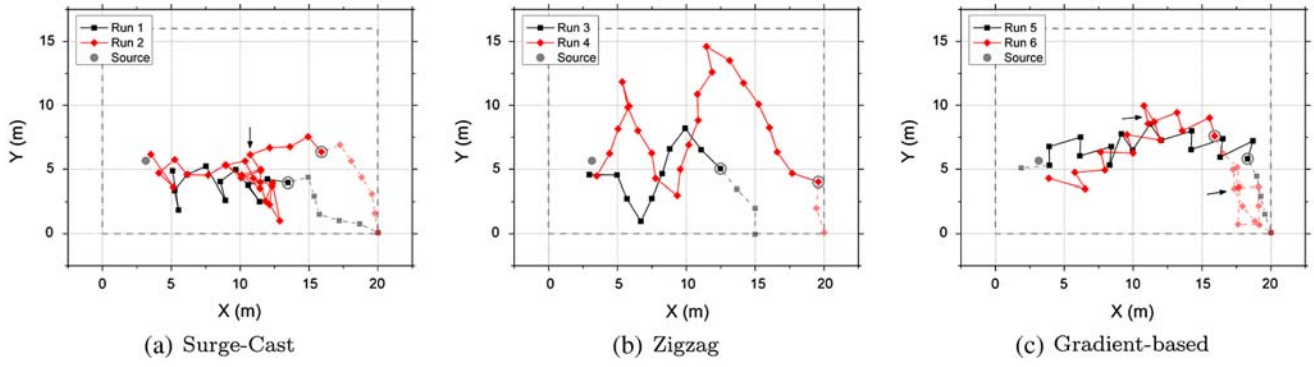

Figure 9. Trajectories of the micro-drone in real-world experiments including the plume acquisition phase. The source position is indicated by the gray point. The gray circles mark the position of the first gas concentration measurements above the threshold. The position, where the wind direction changed in the amount of up to 180° is indicated with black arrows. (For the colour version of this figure, please see the online article: http://dx.doi.org/10.1080/01691864.2013.779052.)

Table 1. Results of the real-world plume tracking experiments (excluding the plume acquisition phase).

	Surge-cast		Zigzag		Gradient-based	
Run	1	2	3	4	5	6
Total #iterations	25	36	17	29	24	38
Travelled distance (m)	21.01	41.78	18.06	44.18	29.65	26.02
Distance overhead d_o (m/m)	2.01	3.27	1.93	2.67	1.96	2.02
Mean	2.64		–		1.99	
95% confidence interval	(1.40, 3.88)		–		(1.93, 2.04)	
PF-localization error (m)	0.73	1.18	0.77	2.86	0.56	0.21
#Neighbors ($r = 0.5$ m)	242	416	224	608	307	604

ent-based). Here, the wind direction varied significantly during the runs precluding the micro-drone to make further progress for some time. This is indicated in Figure 9 with black arrows. However, the overlapping confidence intervals, the small number of experiments, the different step sizes and upwind angles for the zigzag algorithm, and the permanent changing structure of the plume (due to changing wind conditions) do not permit to make a complete statistical evaluation of the algorithms.

Table 1 shows also the results of PF-based GSL algorithm. Although the plume tracking experiments were stopped directly after the micro-drone passed the source, the algorithm was able to locate the gas source with a success rate of 83.3% (five of six trials succeeded). Measurements behind the gas source would have been advantageous to obtain a more accurate and reliable gas source location estimate. However, an average error of successful localizations of 0.69 ± 0.35 m (the average localization error is 1.05 ± 0.94 m) could be obtained. This result is very good considering, e.g., the positioning system error of the micro-drone (± 1.17 m) and is in line with the simulation results presented in Section 5, where the success rate was 86% and the average localization error was 0.96 ± 1.01 m (the average error of successful localizations was 0.62 ± 0.37 m).

7. Conclusions

In this article, we describe a prototype of a gas-sensitive micro-drone, including the possibility to estimate wind vectors without a dedicated anemometer using only the micro-drone's on-board sensors. Next, this work provides an integral solution to the GSL task by including gas source declaration, for a gas-sensitive micro-drone using a novel PF-based GSL approach. Three bio-inspired plume tracking algorithms and their implementation for a gas-sensitive micro-drone were described, including a new measuring strategy especially designed for, but not limited to, a micro-drone.

The performance of the presented algorithms was evaluated successfully in simulation experiments and tested in real-world experiments. The results of the real-world experiments demonstrate that plume tracking with a gas-sensitive micro-drone can be done under particular environmental conditions. The micro-drone was able to reacquire the plume even during periods of strongly changing wind. The initial results from the real-world experiments indicate that the pseudo-gradient-based algorithm is at least as efficient as the surge-cast algorithm. A good correlation between the results from simulation and real-world experiments can be found for the pseudo-gradient-based algorithm and the zigzag algorithm. Thus, regarding the current implementation of the surge-cast algorithm, the pseudo-gradient-based algorithm and the zigzag algorithm (with larger upwind angle) are the most promising algorithms to use with the micro-drone.

The meta-parameters of the PF-based GSL algorithm were optimized successfully in robotic simulations in order to find an optimal parameter set for the gas-sensitive micro-drone. Furthermore, the real-world results indicate the potential of the proposed PF-based GSL approach for accurately localizing a single gas emission source emitting a known chemical compound in turbulent outdoor environments with a gas-sensitive micro-drone.

Although it was shown that plume tracking is possible under certain circumstances in the real-world, it is difficult to locate gas sources in scenarios with changing wind conditions and high turbulence. In [21], we demonstrate the weakness of algorithms that directly mimic insect behavior. However, a possible application could be to locate the origin of a pollution caused by, e.g., industrial chimneys in a higher atmospheric layer, where the airflow is more stable, or on wide open landfill sites, geodynamically active regions, waste disposals, and CCS areas.

For simplification, several parameters of the PF-based algorithm were set heuristically to decrease the complexity of the problem. Future work should include the optimization of these parameters. The PF-based algorithm gives ample room for improvements, e.g., the PPE could be classified in even more regions to discriminate between particles which are located far away from the

measuring position and those which are located in the immediate vicinity. Future work should also include to run large test sets with different wind and weather conditions on, e.g., wide open landfill sites to obtain the performance and robustness of these algorithms in natural environments. A general extension of this work would be to adapt these methods for the third dimension and a sophisticated multirobot collaboration scheme may help to reduce the time needed to cover larger areas.

Acknowledgments

The authors thank the participating colleagues from BAM and Örebro University. They also express their gratitude to BMWi (MNPQ Program; file number 28/07) and Robotdalen (Gasbot; project number 8140) for funding the research.

Notes on contributors

Patrick P. Neumann is a scientist at BAM Federal Institute for Materials Research and Testing in the division 8.1 Sensors, Measurement and Testing Methods, Germany, since 2008. He has a diploma degree (Dipl.-Inf.) in Computer Science from the Freie Universität Berlin, Germany. Currently, he is graduating in the field of robotics (direction: mobile robot olfaction). His PhD thesis addresses gas source localization and gas distribution mapping with a micro-drone.

Victor Hernandez Bennetts is a PhD student at the AASS research center, Örebro University. In 2010, he obtained a MSc in Robotics and Intelligent Systems from Örebro University. His MSc thesis addresses gas discrimination with a temperature-modulated array of metal oxide gas sensors. He received his bachelor degree (2003) from the Technological University of the Mixteca in Oaxaca, Mexico.

Achim J. Lilienthal is an associate professor at the AASS Research Center at Örebro University, Sweden, where he is leading the Mobile Robotics and Olfaction Lab. His main research interests are mobile robot olfaction, rich 3D perception, robot vision, and safe navigation for autonomous transport robots. He obtained his PhD in computer science from Tübingen University, Germany, and his MSc and BSc in Physics from the University of Konstanz, Germany. His PhD thesis addresses gas distribution mapping and gas source localization with a mobile robot.

Matthias Bartholmai is senior scientist of BAM Federal Institute for Materials Research and Testing, and deputy head of the division 8.1 Sensors, Measurement and Testing Methods. He graduated in energy and process engineering at the Technical University of Berlin and received a PhD in the field of flame protection of polymers. His actual range of activity is the development, validation, and application of innovative measuring systems and sensor technologies with focus on multisensor technologies, distributed sensing, and remote sensing.

Jochen H. Schiller is head of the working group Computer Systems & Telematics at the Institute of Computer Science, Freie Universität Berlin, Germany. His research focus is on wireless, mobile, and embedded devices, communication protocols, operating systems for devices with small footprint, and quality of service and security aspects in communication systems. Up to now, he published five books and more than 150 international papers.

References

[1] Cardé R, Willis M. Navigational strategies used by insects to find distant, wind-borne sources of odor. J. Chem. Ecol. 2008;34:854–866.

[2] Kowadlo G, Russell RA. Robot odor localization: a taxonomy and survey. Int. J. Rob. Res. 2008;27:869–894.

[3] Kuwana Y, Nagasawa S, Shimoyama I, Kanzaki R. Synthesis of the pheromone-oriented behaviour of silkworm moths by a mobile robot with moth antennae as pheromone sensors. Biosens. Bioelectron. 1999;14:195–202.

[4] Grasso FW, Consi TR, Mountain DC, Atema J. Biomimetic robot lobster performs chemo-orientation in turbulence using a pair of spatially separated sensors: progress and challenges. Rob. Auton. Syst. 2000;30:115–131.

[5] Russell R, Bab-Hadiashar A, Shepherd R, Wallace G. A comparison of reactive chemotaxis algorithms. Rob. Auton. Syst. 2003;45:83–97.

[6] Vergassola M, Villermaux E, Shraiman BI. 'Infotaxis' as a strategy for searching without gradients. Nature. 2007;445:406–409.

[7] Shraiman BI, Siggia ED. Scalar turbulence. Nature. 2000;405:639–646.

[8] Lochmatter T. Bio-inspired and probabilistic algorithms for distributed odor source localization using mobile robots [PhD thesis]. EPFL, Lausanne, Switzerland, February 2010.

[9] Ishida H, Suetsugu K, Nakamoto T, Moriizumi T. Study of autonomous mobile sensing system for localization of odor source using gas sensors and anemometric sensors. Sens. Actuators A. 1994;45:153–157.

[10] Bartholmai M, Neumann P. Adaptive spatial-resolved gas concentration measurement using a micro-drone. TM – Technisches Messen. 2011;78:470–478.
[11] Neumann P, Asadi S, Lilienthal AJ, Bartholmai M, Schiller J. Autonomous gas-sensitive microdrone: wind vector estimation and gas distribution mapping. IEEE Rob. Automat. Mag. 2012;19(1):50–61.
[12] Braitenberg V. Vehicles: experiments in synthetic psychology. Cambridge (MA): The MIT Press; 1984.
[13] Lilienthal A, Duckett T. Experimental analysis of gas-sensitive Braitenberg vehicles. Adv. Rob. 2004;18:817–834.
[14] Hayes A, Martinoli A, Goodman R. Distributed odor source localization. IEEE Sens. J. 2002;2:260–271.
[15] Li W. Moth plume-tracing derived algorithm for identifying chemical source in near-shore ocean environments. In: IEEE/RSJ International Conference on Intelligent Robots and Systems; 2007; San Diego, California, USA. p. 2162–2167.
[16] Li J-G, Meng Q-H, Wang Y, Zeng M. Odor source localization using a mobile robot in outdoor airflow environments with a particle filter algorithm. Auton. Rob. 2011;30:281–292.
[17] Williams E. Aviation formulary V1.46. [cited 2011 Apr]. Available from: http://www.williams.best.vwh.net/
[18] Liu J, Chen R, Logvinenko T. A theoretical framework for sequential importance sampling and resampling. In: Sequential Monte Carlo methods in practice. New York: Springer Verlag; 2001. p. 225–242.
[19] Pashami S, Asadi S, Lilienthal AJ. Integration of Openfoam flow simulation and filament-based gas propagation models for gas dispersion simulation. In: Proceedings of the Open Source CFD International Conference; 2010; Munich, Germany.
[20] Lilienthal A, Duckett T. A stereo electronic nose for a mobile inspection robot. In: Proceedings of the IEEE International Workshop on Robotic Sensing (ROSE); 2003; Örebro, Sweden. IEEE.
[21] Bennetts VH, Lilienthal AJ, Neumann P, Trincavelli M. Mobile robots for localizing gas emission sources on landfill sites: is bio-inspiration the way to go? Frontiers Neuroeng. 2012;4:1–12.